XMM-Newton observations of MBM 12: More constraints on the Solar Wind Charge Exchange and Local Bubble emissions

Dimitra Koutroumpa[1], Randall K. Smith[2], Richard J. Edgar[2], Kip D. Kuntz[3], Paul P. Plucinsky[2], and Steven L. Snowden[1]

ABSTRACT

We present the first analysis of an *XMM-Newton* observation of the nearby molecular cloud MBM 12. We find that in the direction of MBM 12 the total O VII (0.57 keV) triplet emission is $1.8^{+0.5}_{-0.6}$ photons cm^{-2} s^{-1} sr^{-1} (or Line Units - LU) while for the O VIII (0.65 keV) line emission we find a 3σ upper limit of <1 LU. We also use a heliospheric model to calculate the O VII and O VIII emission generated by Solar Wind Charge-eXchange (SWCX) which we compare to the *XMM-Newton* observations. This comparison provides new constraints on the relative heliospheric and Local Bubble contributions to the local diffuse X-ray background. The heliospheric SWCX model predicts 0.82 LU for O VII, which accounts for ~46±15% of the observed value, and 0.33 LU for the O VIII line emission consistent with the *XMM-Newton* observed value. We discuss our results in combination with previous observations of the MBM 12 with *CHANDRA* and *Suzaku*.

Subject headings: X-rays: observations — X-rays: diffuse background — Solar System — ISM: bubbles supernovae remnants

1. Introduction

The major sources of the Soft X-ray Background (SXRB) below 1 keV, besides distinct structures such as supernovae and superbubbles (e.g., Loop I), are: absorbed extragalactic emission (primarily unresolved AGN), an absorbed thermal component from the Galactic disk and halo, an unabsorbed thermal component attributed to gas in the Local Hot Bubble (LHB) and the recently identified unabsorbed Solar Wind Charge-eXchange (SWCX) emission from the heliosphere and the geocorona.

Absorption measurements towards nearby stars show that the Sun is surrounded by a large (r ~ 100 pc) low-density region, sometimes called the Local Cavity (Cox & Reynolds 1987). Part of this cavity may be filled with hot gas, forming the so called 'Local Hot Bubble'. This idea derived from the need to explain the fraction of the soft X-ray background that does not anticorrelate with the interstellar column density, and thus can not be attributed to distant Galactic emission, although its distribution in the sky seems to align with Galactic, and not ecliptic, coordinates (Sanders et al. 1977; Snowden et al. 1990). The temperature of the emitting gas has been inferred by the Wisconsin (Fried et al. 1980; McCammon & Sanders 1990; Snowden et al. 1990) and *ROSAT* (Snowden 1993) surveys band ratios in the $\frac{1}{4}$ keV energy range, and found to be around 10^6 K (0.1 keV). The Cosmic Hot Interstellar Plasma Spectrometer (CHIPS: Hurwitz et al. 2005) did not detect the far-ultraviolet (FUV) emission expected from surrounding 10^6 K gas, and placed the LHB temper-

[1]Code 662, NASA/Goddard Space Flight Center, Greenbelt, MD 20771, USA

[2]Harvard - Smithsonian Center for Astrophysics, Cambridge, MA 02138, USA

[3]Henry A. Rowland Department of Physics and Astronomy, The Johns Hopkins University, Baltimore, MD 21218, USA

ature rather at 0.086 keV for an emission measure of 4×10^4 cm^{-6} pc.

SWCX X-ray emission in the heliosphere originates when a high charge state ion of the solar wind interacts with a neutral atom and gains an electron in a highly excited state which then decays by emission of one or more X-rays. Since SWCX X-ray emission was first discovered in observations of comets (Lisse et al. 1996), it was also confirmed to occur in the near-Earth environment where the neutrals are exospheric material in and near the magnetosheath (e.g., Cravens et al. 2001; Snowden et al. 2009), and throughout the solar system where the target atoms are from the interstellar medium (Cox 1998; Cravens 2000). The two later components (and especially the heliospheric emission) create a diffuse 'foreground' emission that is present in every X-ray observation. This diffuse emission is strongly dependent on the solar wind proton flux and heavy ion abundances. However its effect on X-ray observations is very difficult to predict, due to the combination of the fast responding geocoronal (because of the small volume of the neutral distribution around the observer) and slowly varying heliospheric components. A characteristic example of a combination of geocoronal and heliospheric SWCX emissions was detected by *XMM-Newton* while observing the Hubble Deep Field-North (Snowden, Collier, & Kuntz 2004).

SWCX emission is thought to comprise a significant part of the diffuse X-ray background observed at energies $\lesssim$ 1 keV. The most explicit signature of SWCX is usually observed in the form of Long-Term Enhancements (LTEs), that were extensively observed and analyzed during the *ROSAT* All-Sky Survey (RASS, e.g. Snowden et al. 1995). However, the relative contribution of the LHB plasma and the quiescent heliospheric SWCX emission to the local (unabsorbed) SXRB has been a vivid subject of debate in the last decade. Models of the heliospheric SWCX emission (e.g. Robertson & Cravens 2003; Koutroumpa et al. 2007) predict that 50 to 100% of the X-ray emission in the $\frac{3}{4}$ keV energy band may be attributed to the heliosphere. In the $\frac{1}{4}$ keV band where the LHB plasma is thought to emit the most, the fraction accounted for by SWCX is more uncertain. Although recent simulations show that the SWCX emission may account for almost all the $\frac{1}{4}$ keV band SXRB at low latitudes ($|b|$ <25°, Koutroumpa et al. 2009b), CX atomic calculations for heavy ions with strong lines in the $\frac{1}{4}$ keV band (such as Fe, Si, S, Mg) are still based on approximations and the results should evolve in the future. At high latitudes, the Koutroumpa et al. (2009b) model predictions are lower than the measured SXRB intensities, and some local emission from the IS medium is needed.

In general, when trying to compare the LHB and SWCX emissions, the contributions of the distant components of the SXRB (Galactic disk & halo, and extragalactic sources) blur the results even more. In order to avoid this complication the usual strategy is to employ shadowing observations, which consist of pointing towards a dense molecular cloud that will absorb more or less efficiently the distant components of the SXRB, leaving only the local components of interest, i.e., the LHB and SWCX emissions.

The perfect candidate for this kind of observing strategy is MBM 12, a nearby high-galactic (l, b $\sim$ 159°, -34°), low-ecliptic (λ, β $\sim$ 47°, 3°) latitude molecular cloud , with a column density of $\sim4\times10^{21}$ cm^{-2} (Smith et al. 2005), which is optically thick for the oxygen lines energies that are of interest in our analysis (optical depths of 3.5 and 2.4 for O VII and O VIII respectively). Early estimates of the distance to MBM 12 were controversial and have placed it between 65 and 360 pc (Hobbs et al. 1986; Andersson et al. 2002). More recent studies, have further constrained its distance to 90-150 pc (Lallement et al. 2003). In any case, the exact distance of MBM 12 is not important, since the cloud is nearer than the non-local sources of the SXRB in the $\frac{3}{4}$ keV band.

Snowden et al. (1993) first observed MBM 12 as an X-ray shadow with *ROSAT* in order to measure the LHB soft X-ray emission in the $\frac{1}{4}$ keV and $\frac{3}{4}$ keV energy bands. They placed a 2σ upper limit of 270 counts s^{-1} sr^{-1} in the *ROSAT* $\frac{3}{4}$ keV band, which includes both the O VII triplet at 0.57 keV and the O VIII Lyman-α line at 0.65 keV. They fitted the $\frac{1}{4}$ keV band data with a standard 10^6 K thermal model assuming a pathlength of $\sim$65 pc and found an emission measure of 0.0024 cm^{-6} pc. This model yields 47 counts s^{-1} sr^{-1} in the $\frac{3}{4}$ keV band, which corresponds to 0.28 photons cm^{-2} s^{-1} sr^{-1}(if we assume that O VII is the dominant contribution

to the $\frac{3}{4}$ keV band emission), hereafter named Line Units (LU). However, *ROSAT*'s lack of spectral resolution within the bands, did not allow the separation of the O VII from the O VIII line emission, the background continuum and possible other spectral features.

Smith et al. (2005) repeated the MBM 12 observations using the *CHANDRA* ACIS instrument in August 2000, but their results were adversely influenced by a strong Coronal Mass Ejection (CME). They measured particularly strong O VII and O VIII line emission with a surface brightness of 1.79±0.55 LU and 2.34±0.36 LU respectively, much larger than Snowden et al. (1993)'s limits. They argued that this intense oxygen line emission could not come from any of the standard LHB models, either equilibrium or strongly recombining, and suggested that their results were contaminated by SWCX. As it turned out, this CME did indeed produce a strong enhancement of SWCX emission in the heliosphere (and possibly the geocorona) as demonstrated by Koutroumpa et al. (2007).

A third observation of MBM 12 was performed with *Suzaku* in February 2006 (Smith et al. 2007). Towards MBM 12, the O VII emission line was detected with a surface brightness of 3.34±0.26 LU, and the O VIII flux was 0.24±0.1 LU. Smith et al. (2007) fitted the data with a standard thermal model and found that the emission could be explained by a region with 100 pc radius, an electron density of 0.0087 cm^{-3}, and a temperature of 1.2×10^6 K. However, these parameters would predict a $\frac{1}{4}$ keV emission in excess of observations.

Using a self-consistent simulation of the heliospheric SWCX emission responding to quasi-real time variations of the solar wind proton flux and heavy ion abundances, Koutroumpa et al. (2007) estimated the heliospheric SWCX emission from the O VII and O VIII lines in the case of both the *CHANDRA* and *Suzaku* observations of the MBM 12. along with two more observations of a high-latitude shadowing filament with *Suzaku* and *XMM-Newton* (for an updated analysis of the filament observations see Henley & Shelton 2008). Arguing for both the short-scale solar wind variations and global solar activity variations due to the 11-year solar cycle, the authors simulated the heliospheric SWCX emission during each of these shadowing observations. They found that almost 100% of the oxygen emission in front of these shadowing clouds may be explained by means of the heliospheric SWCX emission alone, and that there was no need for emission from gas in the LHB in these directions. This work presents another step in the continuing effort to confirm these results.

In this paper we present the first analysis of an MBM 12 observation with *XMM-Newton* and compare the results with a model used to calculate the heliospheric SWCX emission, in order to place more constraints on the contribution of the heliospheric and LHB gas emissions to the local diffuse SXRB. The paper is organized as follows: In Section 2 we present the *XMM-Newton* data analysis and results. In Section 3 we describe the heliospheric SWCX simulations and results for the period and LOS of the MBM 12 observation. Finally, in Section 4 we compare the SWCX model results to the X-ray data and discuss the implications on the local diffuse X-ray background, in combination with results from previous observations towards the MBM 12 and other shadowing fields.

2. X-Ray Observations

The molecular cloud MBM 12 was observed by *XMM-Newton* on several occasions (typically in February and August) from 2000 to 2008 for a total of 131.1 ks (Observation IDs: 0110660101, 0112510301, 0501370101, 0501370201 & 0552920101). The pointing positions were distributed around a region roughly centered at (RA, Dec) ~ 02h55m58s, +19°28'19" (J2000) (l, b = 159.2°, -34.5°; λ, β ~ 47°, +3°). Of these observations, the first four were badly contaminated by the soft proton background, and only the last one (ID#0552920101) was used in this analysis. The observation took place on August 12, 2008 for a total exposure of ~35 ks (see observation details in Table 1).

We reduced the EPIC data using the *XMM-Newton* ESAS[1] analysis package (Snowden & Kuntz 2006) as demonstrated in Snowden et al. (2008). The data were first filtered for excesses in the normal internal particle background and for contamination by soft protons (Kuntz & Snowden 2008a). Next, data from the full field of view were

[1] http://heasarc.gsfc.nasa.gov/docs/xmm/xmmhp_xmmesas.html

Table 1: *XMM-Newton* MBM 12 Observation Details

Obs ID	Start Date	Exposure	Good Time
0552920101	2008-08-12 18:30:55	34.9 ks	22.2 ks (MOS1) 24.6 ks (MOS2) 12.2 ks (PN)
Line Fluxes in LU			
Fitted		SWCX Model	
O VII Flux	O VIII Flux	O VII Flux	O VIII Flux
$1.8^{+0.5}_{-0.6}$	<1.00	0.82	0.33

extracted after the exclusion of point sources. Finally model particle background spectra were produced for subtraction during the spectral fitting process.

In Figure 1 we present the spectral fit for the *XMM-Newton* MBM 12 data. The spectra were fit with XSPEC, using a model which included two thermal components (an unabsorbed $\sim$ 0.1 keV Raymond-Smith model for local emission and an absorbed $\sim$ 0.23 keV APEC model for the more distant disk and halo emission), an absorbed power law representing the cosmic background with a spectral index of 1.3, monochromatic lines at 1.49 keV and 1.75 keV representing the internal fluorescent Al Kα and Si Kα background, and a power law not folded through the instrumental response representing any residual soft proton contamination left after the screening process. In the thermal spectral models we set the abundance of oxygen to zero and the other abundances were fixed at 1 (based on the assumption that oxygen will dominate any SWCX emission in the *XMM-Newton* bandpass). We then added two monochromatic lines at 0.57 keV and 0.65 keV to the model to represent the observed oxygen emission from both SWCX and more distant cosmic emission, the latter which produces a constant contribution. The absorption of the halo thermal components and the power law were allowed to float and the best fit value for the column density was $N_H = (7\pm2)\times10^{21}$ cm^{-2}, which is in good agreement with the 4×10^{21} cm^{-2} from Smith et al. (2005). A spectrum derived from the RASS data was simultaneously fit, with the oxygen emission coming from the thermal models rather than the monochromatic lines, in order to constrain the low-temperature thermal component. All of the data were fit simultaneously allowing only the SWCX oxygen Gaussian energies and normalizations, instrumental Al and Si Gaussians, and soft-proton power law components to vary. The fit is reasonably good for the cosmic background with a χ^2_ν value of 1.35 for 835 d.o.f. The best fit for the O VII line energy was found at 554^{+10}_{-6} eV, with a line flux equal to $1.8^{+0.5}_{-0.6}$ LU. The best fit result for O VIII is a marginal detection of the feature with surface brightness $0.56^{+0.24}_{-0.46}$ LU, which allows us only to place a 3σ limit of <1 LU for the O VIII line flux. The fitted O VII and O VIII line fluxes are listed in Table 1.

3. Heliospheric SWCX simulations

The heliospheric SWCX model we use for our simulations is a self-consistent calculation of the SWCX line emission, based on 3-dimensional grids of the IS neutral species (H and He) distributions in the heliosphere modulated by solar activity (gravity, radiation pressure, and ionization processes) and 3-dimensional density distributions of the highly charged heavy solar wind (SW) ions taking into account their radial propagation and their partial depletion due to CX reactions with the IS neutrals. This model has been extensively described in Koutroumpa et al. (2006, 2007), and detailed information on the IS neutral and SW input parameters for different periods of the solar cycle were provided in Koutroumpa et al. (2009) based on references therein. With this model we can calculate complete spectra of the SWCX emission in any direction in the heliosphere for any date, using photon emission yields computed by Kharchenko & Dalgarno (2000) for all ion spectral lines following CX with the corresponding neu-

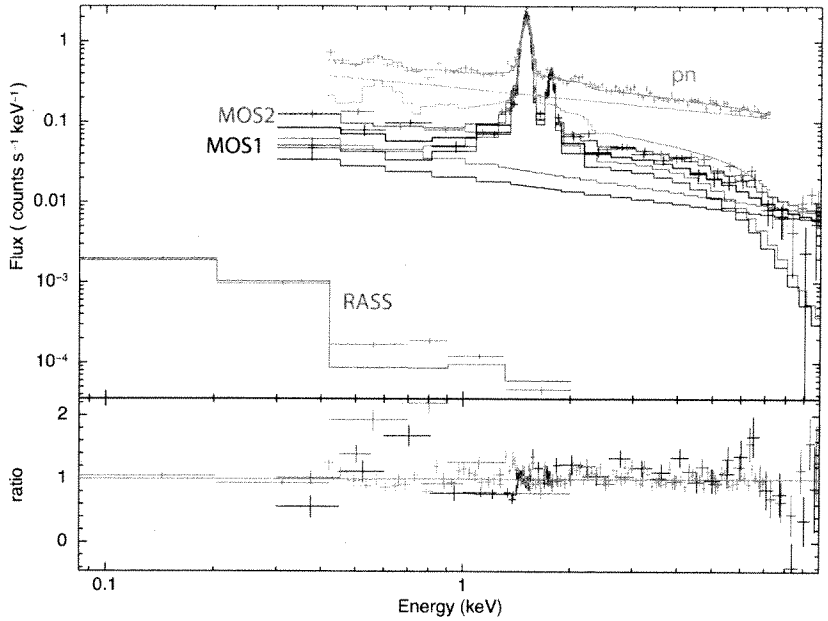

Fig. 1.— The upper set of data and curves (green) are the PN spectra, the middle set of data and curves are the MOS1 (black) and MOS 2 (red) spectra, and the bottom (blue) is the RASS spectrum. [*See the electronic edition of the Journal for a color version of this figure.*]

tral species (H and He individually). However, for comparison to present X-ray observations we use the O VII triplet at 0.57 keV and the O VIII line at 0.65 keV, as they are the strongest spectral features and provide the best signal-to-noise ratio for the observations.

In Koutroumpa et al. (2007) we introduced a dynamic variant of the model that we also use here in order to simulate quasi-real time SW variations and their influence on the heliospheric component of the SWCX emission on the MBM 12 LOS during the *XMM-Newton* observation. Of note however, the model does not account for SWCX emission from the geocorona and is unable to predict the near-earth environment reactions to the SW stimulus.

3.1. Solar wind data input

The *XMM-Newton* observations took place in August 2008 when solar activity was at its minimum phase. In general, during the solar minimum, the quiescent SW flow (outside particularly violent events, e.g. CMEs) has a very distinct highly anisotropic distribution, with a narrow equatorial zone (within $\pm 20^\circ$ of the solar equatorial plane) of slow SW ($\sim$ 400 km s^{-1}), and the fast SW ($\sim$ 700 km s^{-1}) emitted from the polar coronal holes. However, recent results either from direct observations of the solar corona or from indirect observations of the solar wind flux (e.g. de Toma et al. 2010; Lallement et al. 2010) show that the slow wind equatorial zone during the minimum phase of Solar Cycle 23 (years 2008-2009) spans to almost twice the latitudinal extent it occupied during the previous Solar Cycle minimum (years 1996-1997). In any case, the MBM 12 LOS points at ecliptic coordinates $(\lambda,\beta) = (47^\circ, +3^\circ)$, therefore it is very close to the ecliptic plane and embedded in the slow SW flow only.

The ionic composition of the two flows can be very different, and the charge-state distributions change as well, with the higher charge-states strongly depleted (or even completely absent, as for example O^{+8}) in the fast solar wind. Typically, in the model we adopt the oxygen relative abundances published in Schwadron & Cravens (2000): $(O^{+7}, O^{+8}) = (0.2, 0.07)$ for the slow wind. That gives a O^{7+}/O^{6+} ratio of the order of 0.3 for the slow SW. However, from Ulysses measurements (see Gupta et al. 2009), we found

that the O^{7+}/O^{6+} ratio in the slow SW equatorial zone during 2008 was at only 35% of its typical average value, which means that O^{7+} was strongly depleted, even in the slow SW.

The global average properties of the SW are at present well known, thanks to many years of monitoring by a large fleet of solar and heliospheric imagers and in-situ instruments. However, these data provide an average estimate of the quiescent SW, and therefore only an estimate of the quiescent SWCX emission. In real time, the SW flux is extremely variable, with a vast distribution of heavy ion abundances. The Advanced Composition Explorer (*ACE*, Stone et al. 1998) and *WIND* (Ogilvie et al. 1995) satellites at the L1 point provide in-situ density and velocity (among other quantities) measurements of various species in the solar wind. Since SWCX emission is proportional to the flux of the solar wind species producing the emission, the *ACE* and *WIND* data can be used to gain insight into the variation of the observed flux.

More recently, the twin *STEREO* (Solar TErrestrial RElations Observatory; Kaiser 2005) spacecrafts were launched in 2006, and are currently evolving in heliocentric orbits slowly drifting away from the Earth - one ahead of Earth in its orbit (*STEREO A*), the other trailing behind (*STEREO B*). Like *ACE* and *WIND*, the *STEREO* observatories are equiped with solar imaging instruments as well as in-situ detectors for monitoring the solar activity and the solar wind. The combination of the four instruments, placed at ~1 AU from the Sun but at different orbital locations, is essential for the studies of the structure and properties of the ambient solar wind.

The two upper panels of Figure 2 show the solar wind proton flux and bulk speed for the MBM 12 observation interval (shown by the vertical lines), measured with *WIND* and *STEREO A* (*STEREO B* data are less relevant to our study since the MBM 12 LOS points ahead in Earth's orbit, see lowest panel of Figure 2). The quiescent level of the SW proton flux during the period of our observations was $\sim 1.8 \times 10^8$ cm^{-2} s^{-1}, somewhat lower than average equatorial slow SW proton fluxes.

WIND detected a strong proton flux enhancement due to a Corotating Interaction Region (CIR) around 21:00 UT on August 8, ~4 days

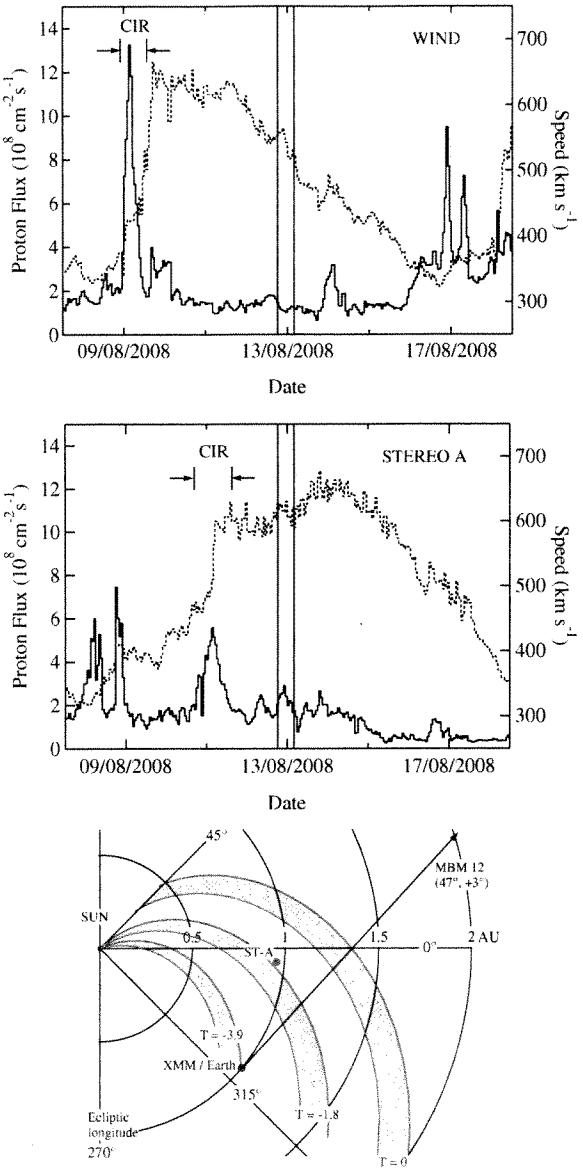

Fig. 2. *Top panel*: Hourly average of the solar wind proton flux (solid line) and average bulk speed (dotted line) from *WIND* for the *XMM-Newton* exposure of MBM 12 (shown by the vertical lines). *Middle panel*: Same as the top panel, only the data are from *STEREO A*. The CIR relevant to the MBM 12 observation is noted both in the *WIND* and *STEREO A* data. *Bottom panel*: Observation geometry for the MBM 12 LOS on August 12, 2008, as seen from the north ecliptic pole. *XMM-Newton*/Earth's and the *STEREO A* spacecraft's positions also shown. *WIND* is positioned at the L1 point in the Sun-Earth direction, but is not marked for clarity. The pink-shaded spirals represent the CIR structure in three 'snapshots': Day T = 0 is the beginning of the *XMM-Newton* observation of the MBM 12, day T = -3.9 is when *WIND* starts detecting the CIR, and day T = -1.8 is approximately the moment *STEREO A* starts detecting the CIR (see text for details). The width of the spirals in radial direction corresponds exactly to the temporal duration of the CIR as measured in the SW instruments. [*See the electronic edition of the Journal for a color version of this figure.*]

before the begining of the *XMM-Newton* MBM 12 observation. A CIR is formed when fast SW (usually from low latitude coronal holes) interacts with slow SW streamers producing a region of compression. The CIR detected with *WIND* was propagating at an average speed of 400 km/s and lasted 16 hours. *STEREO A* measured the same CIR starting about 2 days later (17:00 UT on August 10). However, the compressed region seems to have relaxed over the travel time between *WIND* and *STEREO A* and the overall CIR structure has expanded (lasting 22 hours) and accelerated by ~100 km/s.

Unfortunately, *ACE* data of the oxygen ions relative abundances O^{+7} and O^{+8} were too scarce over the observation period to directly determine the O^{+7} and O^{+8} abundances. Averages over one month before and after the *XMM-Newton* observation show very little O^{+7} (8%) and O^{+8} (1.5%) present in the equatorial wind measured at L1. Therefore, we assume average O^{+7} and O^{+8} abundances at ~45% of their typical values, based on the previously-mentioned Ulysses (and *ACE*) measurements.

3.2. Results

In the lower panel of Figure 2 we show the structure and propagation of the CIR as calculated in the dynamic model. In the model, the SW enhancement is simulated as a step function of the same duration as the CIR and a maximum solar proton flux averaged over the CIR structure. Day T = 0 in the simulation is the start date/time of the *XMM-Newton* MBM 12 observation. The CIR is first observed with *WIND* on T = -3.9 for 16 hours, with an average speed of 400 km/s and an average proton flux of 6.2×10^8 cm^{-2} s^{-1} (used in the step function). In order to simulate as faithfully as possible the travel time between *WIND* and *STEREO A* we used a constant acceleration of 52.6 km/s/day to the final velocity (~500 km/s) measured in *STEREO A* on approximately day T = -1.8. From that moment on, we assume a constant velocity of 500 km/s and a proton flux of 3.5×10^8 cm^{-2} s^{-1}, lasting for 22 hours.

In Figure 3 we present the predicted lightcurves of the O VII and O VIII SWCX emission under the influence of the CIR propagation along the MBM 12 LOS, taking into account the depleted O^{+7} and O^{+8} ion distributions. As Figure 3 shows, the timing between the CIR crossing of the MBM 12 LOS and the begining of the *XMM-Newton* observation reduces the actual influence of the CIR enhancement on the heliospheric SWCX emission to a statistically insignificant effect with respect to the quiescent SWCX level during the same period. Also, from the observation geometry and propagation of the CIR on the LOS, we may conclude that during the *XMM-Newton* observation the SW disruption was well beyond the geocorona ($r \gtrsim 0.7$ AU from the Earth in the MBM 12 direction), and very little SWCX emission should be produced in the near-earth environment. However, we caution that our simulations do not include modeling of the geocoronal SWCX emission, and we cannot conclusively verify this hypothesis.

The line fluxes predicted by the SWCX simulations are 0.82 LU and 0.33 LU for O VII and O VIII respectively. If we assume that the O VII triplet is the dominant contribution to the *ROSAT* $\frac{3}{4}$ keV band, then the model yields ~137 counts s^{-1} sr^{-1}. If we also add the O VIII SWCX line emission, the total flux is estimated to ~193 counts s^{-1} sr^{-1} in the $\frac{3}{4}$ keV band. Both these values are well within the 2σ upper limit measured in the *ROSAT* $\frac{3}{4}$ keV band (Snowden et al. 1993). The SWCX model predictions for the O VII and O VIII line fluxes for the period of the *XMM-Newton* observation are also listed in Table 1.

4. Discussion and Conclusions

We have presented the first spectral analysis of the soft X-ray background emission towards the MBM 12 with *XMM-Newton*. The spectral fit yielded a O VII triplet surface brigthness of $1.8^{+0.5}_{-0.6}$ LU, and placed a 3σ upper limit of <1 LU to the O VIII line emission. We also performed a simulation of the heliospheric SWCX emission towards the same direction for the same observing period. The heliospheric SWCX model predicts 0.82 LU for O VII, which accounts for ~46±15% of the observed value. For comparison, the LHB prediction is 0.28 LU, as noted previously. The model prediction for the O VIII line flux is 0.33 LU which lies well within the upper limit.

In theory, SWCX emission exhibits very distinct spectral characteristics with respect to thermal plasma emission. For instance, the line intensity ratios (forbidden, intercombination and

resonance lines) in triplets of the He-like ions O VII and Ne IX are very different and could be used as spectral diagnostics to separate the two mechanisms (e.g., Lallement 2009, and references therein). While thermal emission has a very strong resonance line (574 eV), SWCX emission favours the forbidden transition (560.9 eV). With the spectral resolution of current missions, though, it is very difficult to distinguish individual SWCX X-rays from those with a more distant origin.

Nevertheless, as noted by Lallement (2009) and applied in Koutroumpa (2009)[2], it is possible to use the apparent displacement in energy of the unresolved O VII gaussian centroid in order to estimate the relative contribution of the individual transitions and thus determine the dominant emission mechanism. It is even best to measure the separation of the O VII and O VIII centroids (the O VIII centroid should be the same for the two mechanisms) in order to minimize the calibration effects of the different instruments in the 0.5-1 keV energy range. However, this approach may also be complicated by the presence of the O VII 3→2 line at 666 eV that is generally difficult to distinguish from the Lyman-α line at CCD resolution. Here, we attempted to measure the fitted O VII and O VIII line energies in order to estimate the contribution of heliospheric SWCX emission towards the MBM 12 cloud and compare to the estimates of the SWCX model. The O VII line energy best fit for this analysis lies at 554^{+10}_{-6} eV and seems consistent with a strong forbidden line that implies an important contamination from SWCX. However as the O VIII line energy could not be constrained with certainty, we cannot draw definite conclusions on the subject.

In Table 2 we summarize the oxygen line fluxes from the recent observations of MBM 12 with *CHANDRA*, *Suzaku*, and *XMM-Newton* along with the heliospheric SWCX model estimates. We also include a list of the foreground oxygen line emission (after subtraction of the absorbed background emission) for four more shadowing observations towards the MBM 20 (Gupta et al. 2009) and the South Galactic Filament (SGF, Henley & Shelton 2008). The SWCX emission estimates for all those observations are derived in the same way as in our present analysis, and have been published in previous works (Koutroumpa et al. 2007; Gupta et al. 2009).

In Figure 4, we present the data versus SWCX model linear fit for the MBM 12 observations (upper panel) and for all the shadowing observations listed in Table 2 (lower panel). For the MBM 12 data the fit to the model gives a correlation coefficient of 0.63±0.2 at 1σ for O VII, while the O VIII data to model fit gives a coefficient of 1.25±0.22 at 1σ (with an intercept of 1.08±0.63 LU and -0.36±0.17 LU for O VII and O VIII respectively). When we include all the shadowing observations data, the correlation is slightly improved both for O VII with a coefficient of 0.65±0.16 (1σ), and for O VIII with a coefficient of 1.2±0.22 (1σ). The intercepts for this fit are 1.07±0.47 LU and -0.34±0.16 LU for O VII and O VIII respectively. This result suggests that although the LHB O VIII is probably negligible, the LHB O VII emission is non-zero in these directions, which is also consistent with Kuntz & Snowden (2008b)'s results that use a similar method.

The model predictions seem to overestimate the O VIII emission, but given the large uncertainties of the heavy SW ion abundance measurements, these predictions remain within the observed errorbars. Thus, we may conclude that the heliospheric SWCX emission may account for all the observed local O VIII background. For O VII, in general, the model predictions suggest that at least as much as half of the observed values are due to SWCX emission from the heliosphere. However, we still consider that the number of shadowing observations that allow a direct comparison of the very local components of the SXRB (i.e. the heliospheric and LHB components) is relatively small, and the statistical significance of this comparison needs to be improved with a larger sample of observations. Also, the heliospheric SWCX simulations are still in progress since they strongly depend on the statistics of the SW input, itself in constant evolution. Hopefully, future missions which will include non-dispersive microcalorimeter spectrometers will be able to separate thermal from SWCX emission using the He-like triplets (e.g. Snowden 2009) and shed more light to the

[2]Accepted *XMM-Newton* AO9 proposal published as a poster presentation at the 'High-resolution X-ray spectroscopy: past, present and future' conference, organized by SRON Netherlands Institute for Space Research and Utrecht University. http://www.sron.nl/files/HEA/XRAY2010/posters/4/4.01_koutroumpa.pdf

TABLE 2

DATA AND MODEL OXYGEN LINE INTENSITIES FOR SHADOWING OBSERVATIONS IN LU

Field Name	Observing Instrument	Data[a] O VII	Data[a] O VIII	SWCX Model O VII	SWCX Model O VIII
MBM 12	*CHANDRA*	1.79±0.55	2.34±0.36	1.49	2.13
	Suzaku	3.34±0.26	0.24±0.10	3.56	0.50
	XMM-Newton	1.8±0.6	<1.00	0.82	0.33
MBM 20	*XMM-Newton*	2.63±0.78	0.03±0.43	1.88	0.74
	Suzaku	0.99±0.91	0.01±1.01	0.15	0.38
SGF	*XMM-Newton*	6.2±2.9		3.16	1.02
	Suzaku	1.1±1.25	1±1.1	0.34	0.02

[a]Foreground emission taking into account the optical depth of the shadows. Data taken from Smith et al. (2005, 2007); Henley & Shelton (2008); Gupta et al. (2009)

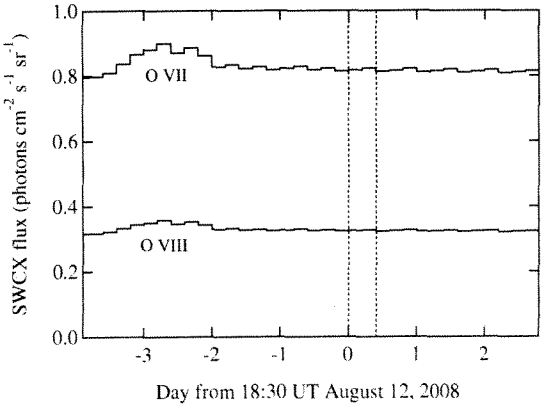

Fig. 3. Lightcurves of the predicted heliospheric SWCX O VII and O VIII line emission during the *XMM-Newton* observation of the MBM 12 on August 12, 2008. The *XMM-Newton* observation interval is marked with the dotted vertical lines.

controversy of the dominant emission mechanism in the local interstellar medium.

Based on observations obtained with *XMM-Newton*, an ESA science mission with instruments and contributions directly funded by ESA Member States and NASA.

We would like to thank the MIT Space Plasma Group (K. W. Ogilvie and A. J. Lazarus) for the WIND data, and the STEREO/PLASTIC Investigation (A. B. Galvin, PI) and NASA Contract NAS5-00132 for the PLASTIC Level 2 data used in this study. We also would like to acknowledge the ACE/SWICS-SWIMS instrument teams (J. Raines, S. Lepri, T. Zurbuchen) and the ACE Science Center for providing the ACE data, and the Ulysses/SWICS team (G. Gloeckler, T. Zurbuchen, R. von Steiger) for the Ulysses/SWICS data.

This research was supported by an appointment to the NASA Postdoctoral Program at the Goddard Space Flight Center, administered by Oak Ridge Associated Universitites through a contract with NASA.

REFERENCES

Andersson, B.-G., Idzi, R., Uomoto, A., Wannier, P. G., Chen, B., & Jorgensen, A. M. 2002, AJ, 124, 2164

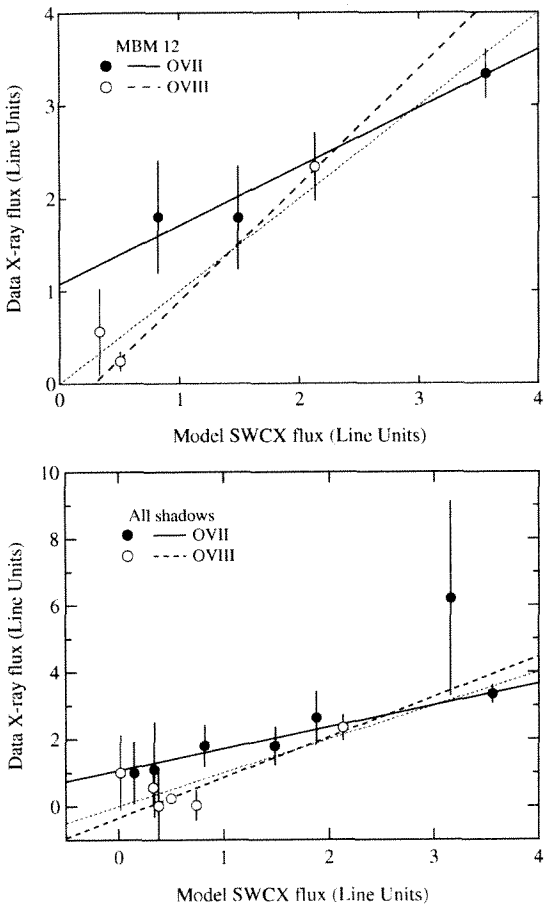

Fig. 4. *Upper panel:* Data versus SWCX model correlation for the 3 most recent on-cloud observations of MBM 12 with *CHANDRA*, *Suzaku* and *XMM-Newton*. The filled circles and plain line represent O VII while the open circles and dashed line stand for O VIII. The grey dotted line traces the y = x line. *Lower panel:* Same as the upper panel, but for all the observations listed in Table 2.

Cox, D. P. 1998, IAU Colloq. 166: The Local Bubble and Beyond, 506, 121

Cox, D. P., & Reynolds, R. J. 1987, ARA&A, 25, 303

Cravens, T. E. 2000, ApJ, 532, L153

Cravens, T. E., Robertson, I. P., & Snowden, S. L. 2001, J. Geophys. Res., 106, 24883

de Toma, G., Gibson, S., Emery, B., & Kozyra, J. 2010, American Institute of Physics Conference Series, 1216, 667

Fried, P. M., Nousek, J. A., Sanders, W. T., & Kraushaar, W. L. 1980, ApJ, 242, 987

Gupta, A., Galeazzi, M., Koutroumpa, D., Smith, R., & Lallement, R. 2009, ApJ, 707, 644

Henley, D. B., & Shelton, R. L. 2008, ApJ, 676, 335

Hobbs, L. M., Blitz, L., & Magnani, L. 1986, ApJ, 306, L109

Hurwitz, M., Sasseen, T. P., & Sirk, M. M. 2005, ApJ, 623, 911

Kaiser, M. L. 2005, Advances in Space Research, 36, 1483

Kharchenko, V., & Dalgarno, A. 2000, J. Geophys. Res., 105, 18351

Koutroumpa, D. 2009, XMM-Newton Proposal ID #06516302, 57

Koutroumpa, D., Collier, M. R., Kuntz, K. D., Lallement, R., & Snowden, S. L. 2009, ApJ, 697, 1214

Koutroumpa, D., Lallement, R., Raymond, J. C., & Kharchenko, V. 2009b, ApJ, 696, 1517

Koutroumpa, D., Acero, F., Lallement, R., Ballet, J., Kharchenko, V. 2007, A&A, 475, 901

Koutroumpa, D., Lallement, R., Kharchenko, V., Dalgarno, A., Pepino, R., Izmodenov, V., Quémerais, E. 2006, A&A, 460, 289

Kuntz, K. D., & Snowden, S. L. 2008, A&A, 478, 575

Kuntz, K. D., & Snowden, S. L. 2008, ApJ, 674, 209

Lallement, R. 2009, Space Science Reviews, 143, 427

Lallement, R., Quémerais, E., Koutroumpa, D., Bertaux, J.-L., Ferron, S., Schmidt, W., & Lamy, P. 2010, American Institute of Physics Conference Series, 1216, 555

Lallement, R., Welsh, B. Y., Vergely, J. L., Crifo, F., & Sfeir, D. 2003, A&A, 411, 447

Lisse, C. M., et al. 1996, Science, 274, 205

McCammon, D., & Sanders, W. T. 1990, ARA&A, 28, 657

Ogilvie, K. W., et al. 1995, Space Science Reviews, 71, 55

Robertson, I. P., & Cravens, T. E. 2003, Journal of Geophysical Research (Space Physics), 108, 8031

Sanders, W. T., Kraushaar, W. L., Nousek, J. A., & Fried, P. M. 1977, ApJ, 217, L87

Schwadron, N. A., & Cravens, T. E. 2000, ApJ, 544, 558

Smith, R. K., Edgar, R. J., Plucinsky, P. P., Wargelin, B. J., Freeman, P. E., & Biller, B. A. 2005, ApJ, 623, 225

Smith, R. K., et al. 2007, PASJ, 59, 141

Snowden, S. L. 1993, Advances in Space Research, 13, 103

Snowden, S. L. 2009, Space Science Reviews, 143, 253

Snowden, S. L., Collier, M. R., & Kuntz, K. D. 2004, ApJ, 610, 1182

Snowden, S. L., Collier, M. R., Cravens, T., Kuntz, K. D., Lepri, S. T., Robertson, I., & Tomas, L. 2009, ApJ, 691, 372

Snowden, S. L., & Kuntz, K. D. 2006, *XMM-Newton* GOF

Snowden, S. L., McCammon, D., & Verter, F. 1993, ApJ, 409, L21

Snowden, S. L., Mushotzky, R. F., Kuntz, K. D., & Davis, D. S. 2008, A&A, 478, 615

Snowden, S. L., Schmitt, J. H. M. M., & Edwards, B. C. 1990, ApJ, 364, 118

Snowden, S. L., et al. 1995, ApJ, 454, 643

Stone, E. C., Frandsen, A. M., Mewaldt, R. A., Christian, E. R., Margolies, D., Ormes, J. F., & Snow, F. 1998, SSRv, 86(1/4), 1

This 2-column preprint was prepared with the AAS LaTeX macros v5.2.